Journal of Cluster Science (2019) 30:203–218
https://doi.org/10.1007/s10876-018-1479-y

ORIGINAL PAPER

A Comparative Computational Investigation of Phosgene Adsorption on $(XY)_{12}$ (X = Al, B and Y = N, P) Nanoclusters: DFT Investigations

Rahman Padash[1,2] · Mehdi Rahimi-Nasrabadi[1,2] · Ali Shokuhi Rad[3] · A. Sobhani-Nasab[4] · Teofil Jesionowski[5] · Hermann Ehrlich[6]

Received: 18 September 2018 / Published online: 28 November 2018

Abstract
In this work, the adsorption of phosgene ($COCl_2$) gas on the outer surface of $Al_{12}N_{12}$, $Al_{12}P_{12}$, $B_{12}N_{12}$ and $B_{12}P_{12}$ pristine nanoclusters is studied with regard to different aspects, including energetic, geometric and electronic properties, using the M06-2X/B97D/B3LYP//6-311g(d,p) levels of theory. The adsorption energies of phosgene molecule on the exterior surface of pure $Al_{12}N_{12}$, $Al_{12}P_{12}$, $B_{12}N_{12}$ and $B_{12}P_{12}$ nanoclusters are − 0.816, − 0.272, − 0.272 and − 0.272 eV, with optimum distances of 2.01, 3.77, 2.52, and 3.42 Å, respectively. Our results show that these combinatorial nanoclusters are able to adsorb the phosgene molecule via exothermic processes. It is demonstrated that by increasing the quantity of phosgene gas, the adsorption energy becomes less negative (except in the case of $Al_{12}P_{12}$). The $Al_{12}N_{12}$ nanocluster is more sensitive to phosgene gas than the other nanoclusters.

Keywords Adsorption · Phosgene gas · Electronic structure · $X_{12}Y_{12}$ Nanocluster

Introduction

Phosgene ($COCl_2$) is a colorless gas with high toxicity, utilized in many industrial applications [1]. It is important in the production of isocyanates, pesticides, pharmaceuticals, engineering plastics, polyurethane materials and military agents, and was used as a chemical weapon in World War I. Phosgene is also used for the production of dimethyl diphenyl urea as a protective gas in the defense industry. Because of its high toxicity, high volatility and low boiling point, the utilization, transportation and storage of phosgene is very dangerous [2]. There have been several theoretical investigations concerning the effective adsorption and detection of phosgene gas, using for example $Al_{12}N_{12}$ [3], Sc-doped BN nanotubes [4], a TiO_2 surface [5], polyaniline nanofiber composites with amines [6] and Al- or Ga-doped $B_{12}N_{12}$ and $B_{16}N_{16}$ nanocages [7]. Elevated concentrations of phosgene in the air can cause pulmonary edema [8]. However, the detection and removal of phosgene molecules using accurate methods and appropriate compounds is a significant new approach.

Due to their high surface-to-volume ratio and spongy surface, nanostructured materials are very appropriate as sensors [9–14]. Also, since the production of fullerenes [15], many researchers have investigated the formation of fullerene and fullerene-related cages as sensors [16, 17]. During the last 20 years, because of their special physical and chemical behaviors and properties and large HOMO–LUMO gap, fullerene-like materials have attracted much attention [18–20]. In computational investigations,

✉ Mehdi Rahimi-Nasrabadi
rahimi@bmsu.ac.ir

✉ Ali Shokuhi Rad
a.shokuhi@gmail.com; a.shokuhi@qaemiau.ac.ir

1 Chemical Injuries Research Center, Systems Biology and Poisonings Institute, Baqiyatallah University of Medical Sciences, Tehran, Iran

2 Faculty of Pharmacy, Baqiyatallah University of Medical Sciences, Tehran, Iran

3 Department of Chemical Engineering, Qaemshahr Branch, Islamic Azad University, Qaemshahr, Iran

4 Young Researchers and Elite Club, Arak Branch, Islamic Azad University, Arak, Iran

5 Institute of Chemical Technology and Engineering, Faculty of Chemical Technology, Poznan University of Technology, Poznan, Poland

6 IESEM, TU Bergakademie, Freiberg, Germany

scientists examined several types of $(XY)_n$ (X = Al, B, … and Y = N, P, …) clusters, and predicted that the fullerene-like cages $X_{12}Y_{12}$ were the most stable [21, 22]. This can be demonstrated in reality: when $n = 12$ the fullerene-like cage $(XY)_n$ may be a favorable cluster and has special intrinsic consistency.

The adsorption properties of various compounds on the outer surfaces of $Al_{12}N_{12}$, $Al_{12}P_{12}$, $B_{12}N_{12}$, and $B_{12}P_{12}$ [23–37] have been investigated in previous studies. For example, Shokuhi Rad et al. studied the adsorption of guanine molecules on the outer surface of four nanocages, utilizing the B3LYP/6-31G(d,p) level of DFT calculations [23]. Even though the adsorption of guanine on $Al_{12}N_{12}$ has the largest adsorption energy, $B_{12}N_{12}$ and $B_{12}P_{12}$ demonstrate more alteration in electronic properties during adsorption of guanine on the nanocages. Also, the interaction of nickel and the surfaces of $Al_{12}P_{12}$ [24] and $Al_{12}N_{12}$ [25] has been investigated. The nickel atom was adsorbed on the outer surface of $Al_{12}P_{12}$ and $Al_{12}N_{12}$ nanoclusters in four different adsorption locations.

Beheshtian et al. investigated the adsorption of CO on the surface of a $B_{12}N_{12}$ nanocage [26]. The adsorption of pyrrole on the surfaces of four $X_{12}Y_{12}$ nanoclusters ($Al_{12}N_{12}$, $Al_{12}P_{12}$, $B_{12}N_{12}$, and $B_{12}P_{12}$) was investigated through density functional theory (DFT) calculations at the B3LYP/6-31G(d,p) level of theory [27].

In this regard, our group explored the interaction of the drug 4-aminopyridine on the outer surface of the above-mentioned semiconductors utilizing the M062x/6-311g(d,p) level of theory [28].

In the present study, our original purpose is to investigate the interaction of phosgene with the outer surface of four pure $X_{12}Y_{12}$ nanoclusters (where X = Al, B, and Y = N, P), using M062x/6-311g(d,p) density functional calculations. Also, structural and electronic properties of the relaxed and complexed nanoclusters of all structures were determined to provide useful information for the outline design of new gas sensors and nanoelectronic apparatus.

Computational Details

In the present work, all nanoclusters contain 24 atoms (donator and acceptor). The initial structures in the presence and absence of phosgene gas were fully optimized using density function theory (DFT). It is significant that the adsorption of phosgene gas on the outer surface of all relaxed nanoclusters is studied with the M06-2X, B3LYP and B97D methods and 6-311g(d,p) basis set. The M06-2X method considers the dispersion forces [38, 39]. Indeed, we use the same computational level of theory for the natural bond orbital (NBO) analysis of all systems. Also, we used the frequency calculations test, at the B3LYP method and 6-311g(d,p) basis set, on the optimized structures to determine the presence of a local minimum on potential energy surface. Here, some of the quantum molecular descriptors [40] such as the ionization potential ($I = -E_{HOMO}$), the electron affinity of the molecule ($A = -E_{LUMO}$), the chemical potential of the system ($\mu = -(I + A)/2$), hardness ($\eta = (I - A)/2$), softness ($S = 1/2\eta$), the electrophilicity index ($\omega = \mu^2/2\eta$) and the Fermi level (E_F) [28] are investigated.

The adsorption energies of the gas on the pristine nanoclusters are calculated via the following equation:

$$E_{ads} = E_{phosgene/nanocluster} - E_{nanocluster} - E_{phosgene} \quad (1)$$

where $E_{phosgene/nanocluster}$, $E_{nanocluster}$ and $E_{phosgene}$ are respectively the total energy of the adsorbed phosgene on the relaxed nanocluster, the total energy of the pure nanocluster and the total energy of the phosgene molecule. To achieve the density of states (DOSs) plot we used the GaussSum program [40]. It should be noted that all theoretical calculations were carried out with the Gaussian 09 program suite [41].

Results and Discussion

Characteristics of $Al_{12}N_{12}$, $Al_{12}P_{12}$, $B_{12}N_{12}$, $B_{12}P_{12}$ and Phosgene

The optimized structure of all pristine nanoclusters (absorbents) and their HOMO and LUMO distributions are presented in Fig. 1. All nanoclusters are built with 6 tetragons and 8 hexagons with two types of X–Y bond among all 36 X–Y bonds; one of them is shared between two hexagons and the other is shared by a hexagon and a tetragon. The X atoms are aluminum and boron and the Y atoms are nitrogen and phosphorus in all nanoclusters. The most important geometric parameters, such as Al–N, Al–P, B–N and B–P bond sizes for all pristine nanoclusters, are shown in this figure. However, to obtain the stability of all structures, the harmonic frequencies for the configurations are performed. Forasmuch as all of the vibrational frequency modes of the configurations are positive (see Table 3), we could conclude that all configurations is optimized on some local minimum.

Our research team calculated the following bond sizes [28]: 1.78 and 1.85 Å (for $Al_{12}N_{12}$), 2.27 and 2.32 (for $Al_{12}P_{12}$), 1.44 and 1.48 (for $B_{12}N_{12}$) and 1.90 and 1.92 (for $B_{12}P_{12}$), for the hexagonal and tetragonal rings respectively, at the M06-2X/6-311g(d,p) level of theory. These are similar to the results reported in [42–47]. The greater strain in the tetragonal rings compared with the hexagonal

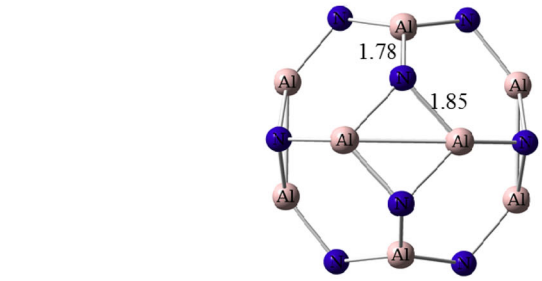

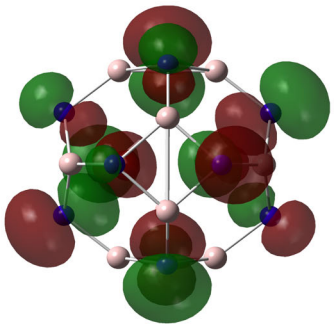

HOMO $Al_{12}N_{12}$

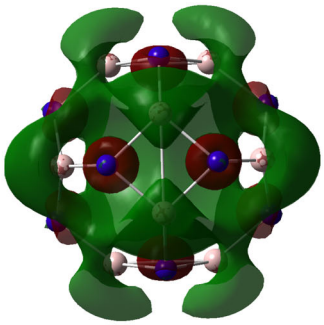

LUMO $Al_{12}N_{12}$

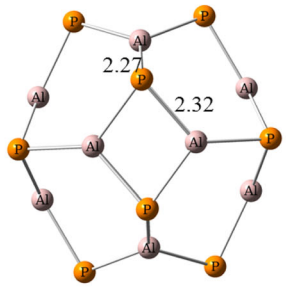

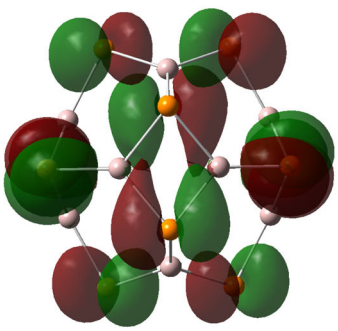

HOMO $Al_{12}P_{12}$

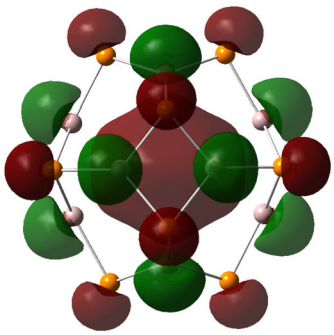

LUMO $Al_{12}P_{12}$

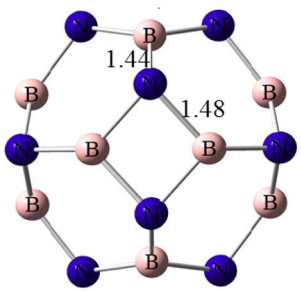

Fig. 1 Relaxed structures of Al12N12, Al12P12, B12N12, B12P12 and phosgene and their HOMO and LUMO distributions. Distances are in Å

Fig. 1 continued

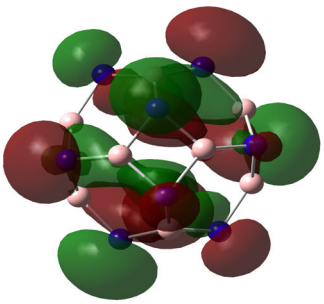

HOMO $B_{12}N_{12}$

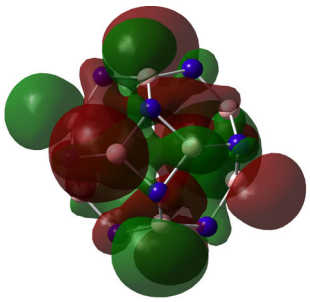

LUMO $B_{12}N_{12}$

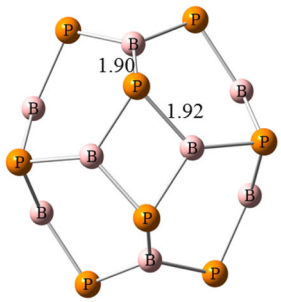

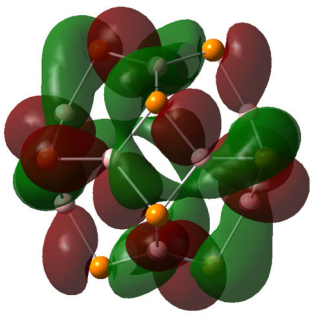

HOMO $B_{12}P_{12}$

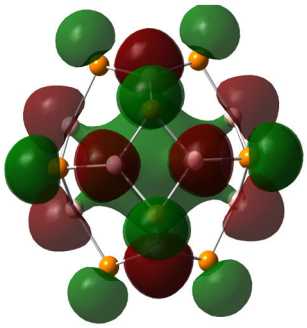

LUMO $B_{12}P_{12}$

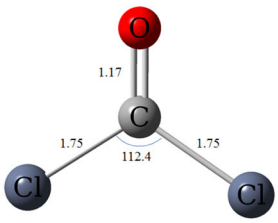

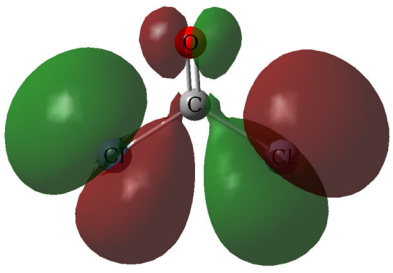

HOMO Phosgene

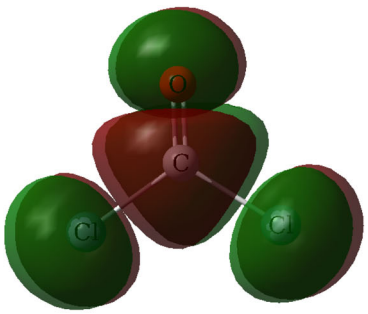

LUMO Phosgene

rings caused the length of the bonds in the tetragonal rings to be greater.

As shown in Table 1, the calculated energies of the HOMO and LUMO levels of $Al_{12}N_{12}$ (and $Al_{12}P_{12}$) and $B_{12}N_{12}$ (and $B_{12}P_{12}$) nanoclusters are − 8.02, − 1.71 (− 7.81, − 3.02) and − 9.44, − 0.01 (− 8.05, − 2.50) eV respectively.

From Table 1, it is quite clear that the energies of the HOMO orbitals of all pure nanoclusters differ significantly from the energies of their LUMO orbitals.

Figure 1 also shows that the HOMO and LUMO profiles are mainly localized on the Y (N and P) atoms and X (Al and B) atoms respectively. Also, the Fermi level energies for $Al_{12}N_{12}$ (and $Al_{12}P_{12}$) and $B_{12}N_{12}$ (and $B_{12}P_{12}$) nanoclusters are − 4.86 (− 5.41) and − 5.32 (− 4.73) eV, and the band gaps are 6.31 (4.79) and 9.43 (5.50) eV respectively.

To calculate E_g (gap energy) for all studied nanoclusters, we used the M06-2X method and the 6-311g(d,p) basis set.

Table 1 HOMO–LUMO gap (E_g) of the $Al_{12}N_{12}$, $Al_{12}P_{12}$, $B_{12}N_{12}$ and $B_{12}P_{12}$ nanocages and phosgene gas calculated using the various level of theory

Property	Phosgene	$Al_{12}N_{12}$	$Al_{12}P_{12}$	$B_{12}N_{12}$	$B_{12}P_{12}$
M06-2X/6-311g(d,p)					
E_{HOMO} (eV)	− 10.81	− 8.02	− 7.81	− 9.44	− 8.05
E_{LUMO} (eV)	− 0.56	− 1.71	− 3.02	− 0.01	− 2.50
E_g (eV)	10.15	6.31	4.79	9.43	5.55
E_F	− 5.68	− 4.86	− 5.41	− 4.72	− 5.27
D_M (Debye)	1.11	0.0	0.0	0.0	0.0
$I = -E_{HOMO}$ (eV)	10.81	8.02	7.81	9.44	8.05
$A = -E_{LUMO}$ (eV)	0.56	1.71	3.02	0.01	2.50
$\eta = (I - A)/2$ (eV)	5.12	3.15	2.39	4.71	2.77
$\mu = -(I + A)/2$ (eV)	− 5.68	− 4.86	− 5.41	− 4.72	− 5.27
$S = 1/2\eta$ (eV^{-1})	0.10	0.16	0.21	0.11	0.18
$\omega = \mu^2/2\eta$ (eV)	3.15	3.75	6.12	2.36	5.01
B97D/6-311g(d,p)					
E_{HOMO} (eV)	− 7.86	− 5.43	− 6.07	− 6.82	− 6.22
E_{LUMO} (eV)	− 2.77	− 3.03	− 3.80	− 1.69	− 3.72
E_g (eV)	5.09	2.40	2.27	5.13	2.5
E_F	− 5.31	− 4.23	− 4.93	− 4.25	− 4.97
D_M (Debye)	0.95	0.0	0.0	0.0	0.0
$I = -E_{HOMO}$ (eV)	7.86	5.43	6.07	6.82	6.22
$A = -E_{LUMO}$ (eV)	2.77	3.03	3.80	1.69	3.72
$\eta = (I - A)/2$ (eV)	2.54	1.2	1.13	2.56	1.25
$\mu = -(I + A)/2$ (eV)	− 5.31	− 4.23	− 4.93	− 4.25	− 4.97
$S = 1/2\eta$ (eV^{-1})	0.20	0.42	0.44	0.20	0.40
$\omega = \mu^2/2\eta$ (eV)	5.22	7.45	10.75	3.53	9.88
B3LYP/6-311g(d,p)					
E_{HOMO} (eV)	− 9.08	− 6.47	− 6.81	− 7.85	− 6.96
E_{LUMO} (eV)	− 1.95	− 2.52	− 3.42	− 1.11	− 3.23
E_g (eV)	7.13	3.95	3.39	6.74	3.73
E_F	− 5.15	− 4.49	− 5.11	− 4.48	− 5.10
D_M (Debye)	1.02	0.0	0.0	0.0	0.0
$I = -E_{HOMO}$ (eV)	9.08	6.47	6.81	7.85	6.96
$A = -E_{LUMO}$ (eV)	1.95	2.52	3.42	1.11	3.23
$\eta = (I - A)/2$ (eV)	3.56	1.97	1.69	3.37	1.86
$\mu = -(I + A)/2$ (eV)	− 5.15	− 4.49	− 5.11	− 4.48	− 5.10
$S = 1/2\eta$ (eV^{-1})	0.14	0.25	0.30	0.15	0.27
$\omega = \mu^2/2\eta$ (eV)	4.26	5.12	7.73	2.98	6.99

All values are in electron volts

Table 2 Ionization potential, electronegativity, electron affinity, chemical potential, softness, hardness, Fermi level, HOMO–LUMO energy gap and electrophilicities of all nanocage/$COCl_2$ complexes

Property	$Al_{12}N_{12}$/phosgene	$Al_{12}P_{12}$/phosgene	$B_{12}N_{12}$/phosgene	$B_{12}P_{12}$/phosgene
M06-2X/6-311g(d,p)				
E_{HOMO} (eV)	− 7.67	− 7.77	− 9.30	− 7.96
E_{LUMO} (eV)	− 2.18	− 3.00	− 0.96	− 2.43
E_g (eV)	5.49	4.77	8.34	5.53
E_{ads}(eV)	− 0.816	− 0.272	− 0.272	− 0.272
D_M (Debye)	5.20	1.14	1.92	1.76
E_F (eV)	− 4.92	− 5.38	− 5.13	− 5.19
$I = -E_{HOMO}$ (eV)	7.67	7.77	9.30	7.96
$A = -E_{LUMO}$ (eV)	2.18	3.00	0.96	2.43
$\eta = (I - A)/2$ (eV)	2.74	3.85	4.17	2.76
$\mu = -(I + A)/2$ (eV)	− 4.92	− 5.38	− 5.13	− 5.19
$S = 1/2\eta$ (eV^{-1})	0.182	0.130	0.120	0.181
$\omega = \mu^2/2\eta$ (eV)	4.42	3.76	3.16	4.88
BSSE(eV)	0.195	0.140	0.092	0.110
B97D/6-311g(d,p)				
E_{HOMO} (eV)	− 5.11	− 6.03	− 6.68	− 6.14
E_{LUMO} (eV)	− 4.07	− 3.77	− 2.96	− 3.65
E_g (eV)	1.04	2.26	3.72	2.49
E_{ads}(eV)	− 0.680	− 0.245	− 0.218	− 0.190
D_M (Debye)	5.09	1.21	1.99	1.46
E_F (eV)	− 4.95	− 4.90	− 4.82	− 4.89
$I = -E_{HOMO}$ (eV)	5.11	6.03	6.68	6.14
$A = -E_{LUMO}$ (eV)	4.07	3.77	2.96	3.65
$\eta = (I - A)/2$ (eV)	0.52	1.13	1.86	1.24
$\mu = -(I + A)/2$ (eV)	− 4.95	− 4.90	− 4.82	− 4.89
$S = 1/2\eta$ (eV^{-1})	0.96	0.44	0.27	0.40
$\omega = \mu^2/2\eta$ (eV)	23.56	10.62	6.24	9.64
B3LYP/6-311g(d,p)				
E_{HOMO} (eV)	− 6.10	− 6.75	− 7.72	− 6.86
E_{LUMO} (eV)	− 3.41	− 3.36	− 2.18	− 3.14
E_g (eV)	2.69	3.39	5.54	3.72
E_{ads}(eV)	− 0.540	− 0.270	− 0.270	− 0.060
D_M (Debye)	5.48	1.65	1.61	1.78
E_F (eV)	− 4.75	− 5.05	− 4.95	− 5.00
$I = -E_{HOMO}$ (eV)	6.10	6.75	7.72	6.86
$A = -E_{LUMO}$ (eV)	3.41	3.36	2.18	3.14
$\eta = (I - A)/2$ (eV)	1.34	1.69	2.77	1.86
$\mu = -(I + A)/2$ (eV)	− 4.75	− 5.05	− 4.95	− 5.00
$S = 1/2\eta$ (eV^{-1})	0.37	0.30	0.18	0.27
$\omega = \mu^2/2\eta$ (eV)	8.42	7.55	4.42	6.72

All parameters are in units of eV

In Table 1, it is shown that the order of the magnitudes of gap energies for all pristine nanoclusters is as follows: $B_{12}P_{12} \gg Al_{12}N_{12} > B_{12}N_{12} > Al_{12}P_{12}$.

The $Al_{12}P_{12}$ and $B_{12}P_{12}$ nanoclusters have respectively the smallest and largest magnitudes of E_g. Hence these are respectively the most and the least electrically conductive nanoclusters. In other words, this means that the $B_{12}P_{12}$ nanocluster behaves more like an insulator than the other nanoclusters. Also, E_g is an indicator of kinetic consistency, and its values show that $Al_{12}P_{12}$ has lower kinetic consistency than the remaining nanoclusters, and thus higher reactivity.

The HOMO and LUMO orbital energies for the phosgene gas are − 10.81 and − 0.56 eV respectively. The E_g

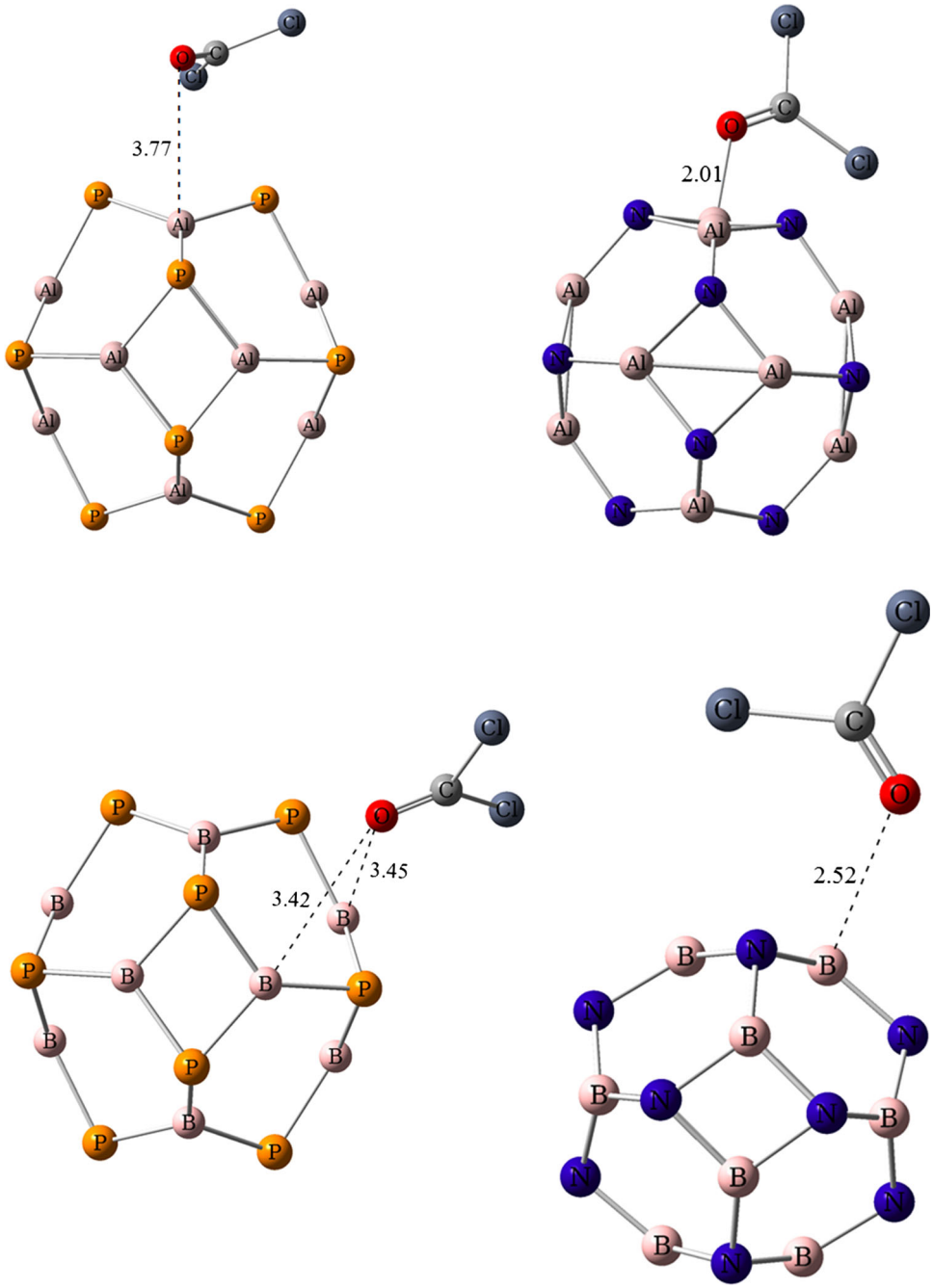

Fig. 2 Optimized structures of phosgene-adsorbed Al12N12, Al12P12, B12N12 and B12P12 complexes. Distances are in Å

value for this molecule is 10.15 eV at M06-2X method. In Tables 1 and 2, it should be noted that this calculated E_g value depends severely on the density functional applied. For instance, using the identical basis set, the B3LYP and B97D functionals give a smaller HOMO–LUMO energy gap than that calculated using the M06-2X method. By comparing the results of various methods in Table 1, we conclude that the results of M06-2X function are better and precise than the other two functions (B3LYP and B97D). This is most likely due to the relatively large contribution of Hartree–Fock exchange energy in the latter density functional, which tends to greatly stabilize the HOMO state [48].

As we expected, the HOMO and LUMO distributions for the phosgene molecule are located in the O, Cl and C atoms respectively. Also, the HOMO distribution in all relaxed nanoclusters is largely located on N and P atoms, while the LUMO distribution is uniformly focused on Al and B atoms. The other important parameters for all pure nanoclusters and phosgene are reported in Table 1.

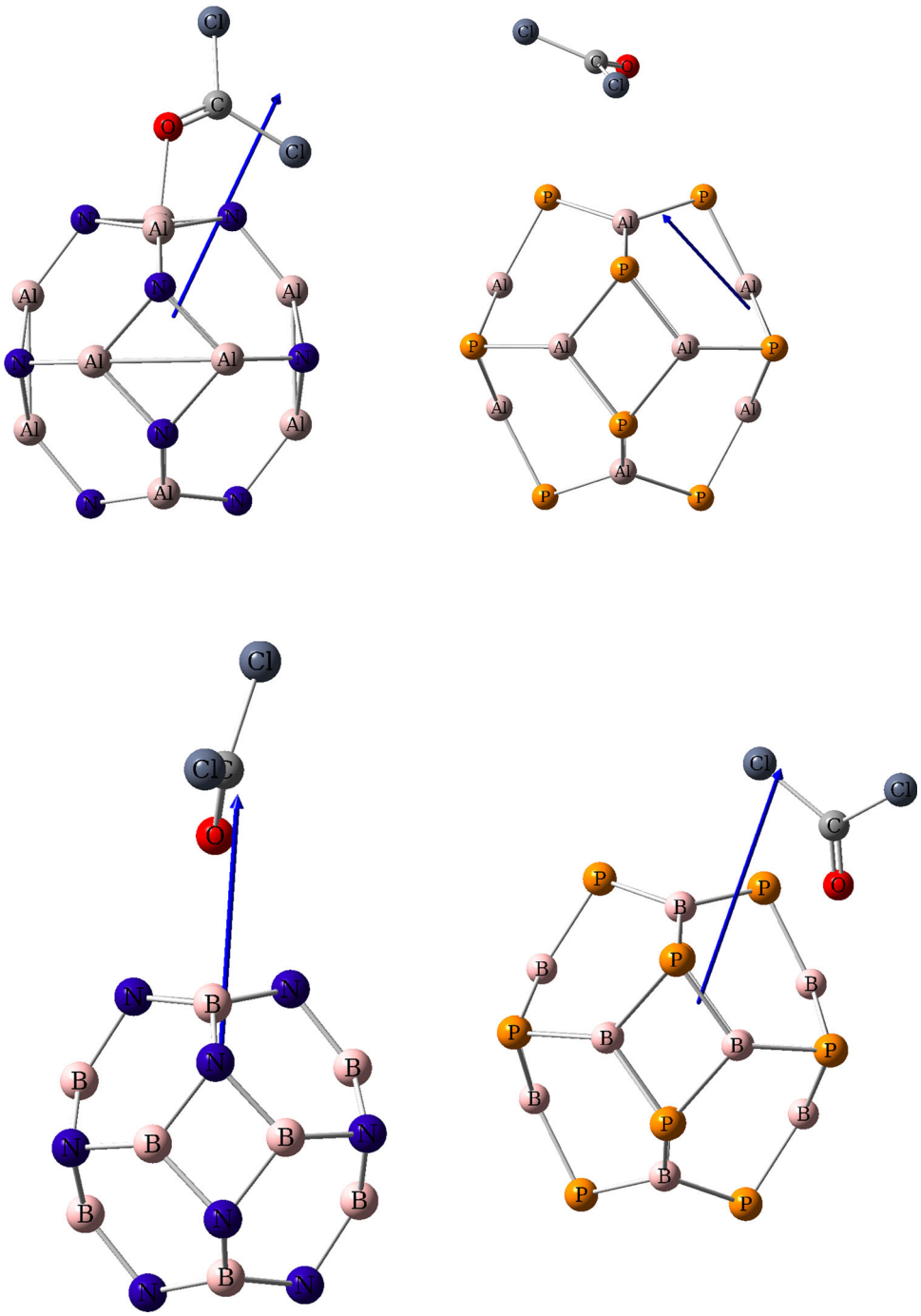

Fig. 3 The dipole moment of each system: Al12N12/phosgene, Al12P12/phosgene, B12N12/phosgene and B12P12/phosgene

Adsorption of Phosgene on $Al_{12}N_{12}$, $Al_{12}P_{12}$, $B_{12}N_{12}$ and $B_{12}P_{12}$

Figure 2 illustrates the adsorption of phosgene gas on the outer surface of relaxed $Al_{12}N_{12}$, $Al_{12}P_{12}$, $B_{12}N_{12}$ and $B_{12}P_{12}$ nanoclusters (Cartesian coordinate of all structures provided in supplementary data file). As can be seen in Fig. 2, when the phosgene gas comes near to the outer surface of any pristine nanocluster, it is adsorbed on the Al atom (for $Al_{12}N_{12}$ and $Al_{12}P_{12}$) or B atom (for $B_{12}N_{12}$ and $B_{12}P_{12}$) of the nanocluster. Upon adsorption of phosgene gas, many significant changes are observed in all nanoclusters. According to the natural bond orbitals (NBOs) analysis, the charge density on Al atoms in $Al_{12}N_{12}$ (and $Al_{12}P_{12}$) nanoclusters which react with one, two and three phosgene molecules are 1.840,1.841 and 1.835e (and 0.921, 0.918, 0.922e), while the charge densities on B atoms in $B_{12}N_{12}$ (and $B_{12}P_{12}$) nanoclusters are 1.230, 1.231, 1.230e (and − 0.131, − 0.141, − 0.131 e), respectively. Also, the distribution of charge density on an

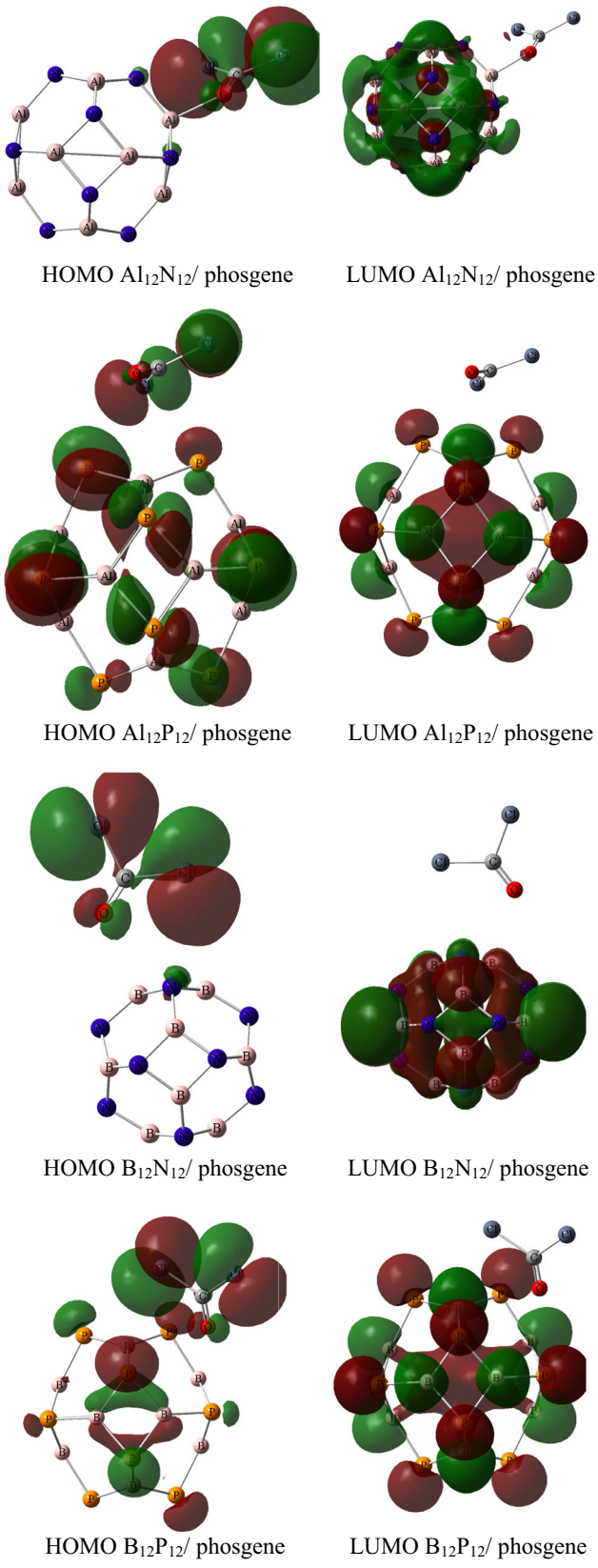

Fig. 4 HOMO and LUMO distributions of phosgene/nanoclusters

oxygen atom, in one, two and three phosgene molecule which reacts with $Al_{12}N_{12}$, ($Al_{12}P_{12}$), and $B_{12}N_{12}$ ($B_{12}P_{12}$) nanoclusters is equal to − 0.564, − 0.561, − 0.557e, (− 0.469, − 0.523, − 0.567e), and − 0.470, − 0.468, − 0.467e, (− 0.490, − 0.489, − 0.476e), respectively. From these numbers, we concluded that with increasing the concentration of phosgene molecule the distribution of charge density do not changed a lot. The higher charge transfer of nitrogen-containing nanocages points towards the higher alters in their electronic structure that is significant for designing a sensor. Comparing pure nanoclusters and nanocluster/phosgene complexes, it is seen that the Al–P, Al–N, B–N and B–P bond sizes change significantly following adsorption. Upon absorption of phosgene gas on the outer surface of all relaxed nanoclusters, all of the bond sizes and angles changed. These variations in the electronic properties generate an electrochemical sensor.

To investigate the ability of all relaxed nanoclusters to sense phosgene gas, some quantum chemical parameters, such as the ionization potential, electronegativity, electron affinity, chemical potential, softness, hardness, Fermi level, HOMO–LUMO energy gap and electrophilicity of all nanocluster/phosgene molecule complexes at different methods are listed in Table 2 and compared with relaxed nanoclusters.

The amounts and separation of charges have a great effect on dipole moment. The adsorption of phosgene gas on the outer surface of relaxed $Al_{12}N_{12}$, $Al_{12}P_{12}$, $B_{12}N_{12}$ and $B_{12}P_{12}$ nanoclusters results in significant change in the dipole moment. For all pure nanoclusters, the dipole moments are essentially zero, whereas after adsorption the magnitudes of the dipole moments increase considerably.

As can be seen in Fig. 3, the magnitudes of the dipole moments of the $Al_{12}N_{12}$/phosgene, $Al_{12}P_{12}$/phosgene, $B_{12}N_{12}$/phosgene, and $B_{12}P_{12}$/phosgene complexes are 5.20, 1.14, 1.92 and 1.76 D, respectively. Finally, for all complexes of nanoclusters with phosgene gas, the dipole moment vectors are directed from the nanocluster towards the phosgene molecule.

The global indexes of reactivity, due to the reactivity and consistency of the phosgene molecules, pristine nanoclusters and complexes, are very important factors. The phosgene molecule is relatively harder (4.21 eV) than all of the studied nanoclusters/phosgene complexes and all relaxed nanoclusters. In other words, following the interaction of the phosgene gas with the exterior surface of all nanostructures, the hardness decreases (except in the case of $Al_{12}P_{12}$). For $Al_{12}N_{12}$ (and $Al_{12}P_{12}$) nanoclusters, the changes in hardness are $\Delta\eta = -0.41$ eV (and $\Delta\eta = 1.4$ eV), while the changes for $B_{12}N_{12}$ (and $B_{12}P_{12}$) are $\Delta\eta = -0.54$ eV (and $\Delta\eta = -0.0$ eV). Softness and hardness are inverse properties; therefore, it is predicted that the softness for all complexes will increase. The changes in

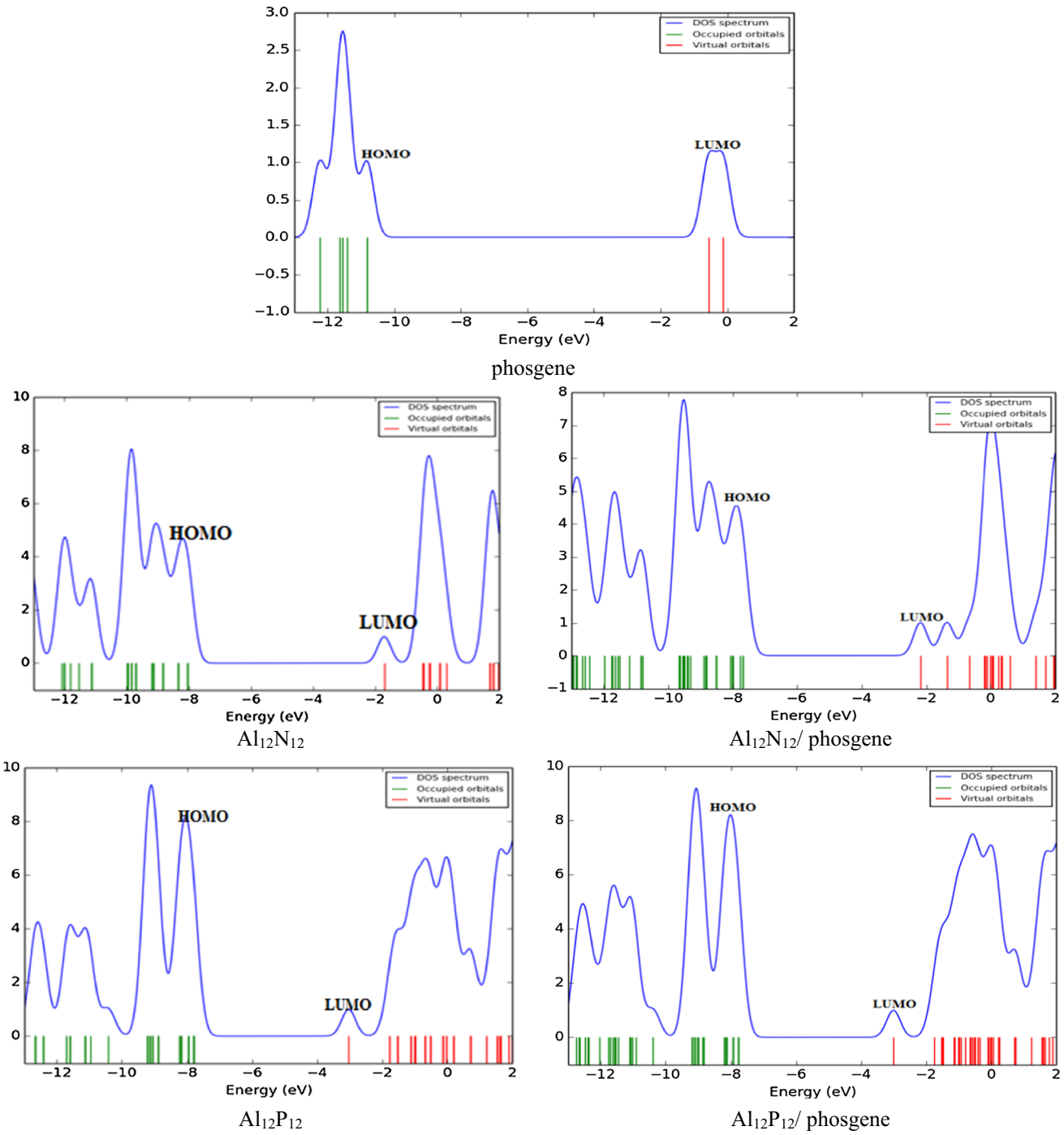

Fig. 5 DOSs of pure and phosgene-adsorbed nanocages

softness following the adsorption of phosgene gas on the exterior surface of $Al_{12}N_{12}$, $Al_{12}P_{12}$, $B_{12}N_{12}$ and $B_{12}P_{12}$ are 0.022, − 0.08, 0.01 and 0.001 eV, respectively.

Generally, complexation between nanoclusters and phosgene molecules raises the chemical potential, but here, for $Al_{12}N_{12}$, the chemical potential changed from − 4.86 to − 4.92 eV. The chemical potentials of $Al_{12}P_{12}$, $B_{12}N_{12}$ and $B_{12}P_{12}$ changed from − 5.41 eV, − 4.72 eV and − 5.27 eV to − 5.38 eV, − 5.13 eV and − 5.19 eV respectively. The greatest and least amounts of variation in chemical potential were obtained for $B_{12}N_{12}$ and $Al_{12}P_{12}$ respectively.

Tables 1 and 2 also give the values of the electrophilicity index ω for isolated nanoclusters and all nanocluster/phosgene complexes. The adsorption of phosgene gas on the outer surface of the nanoclusters led to higher

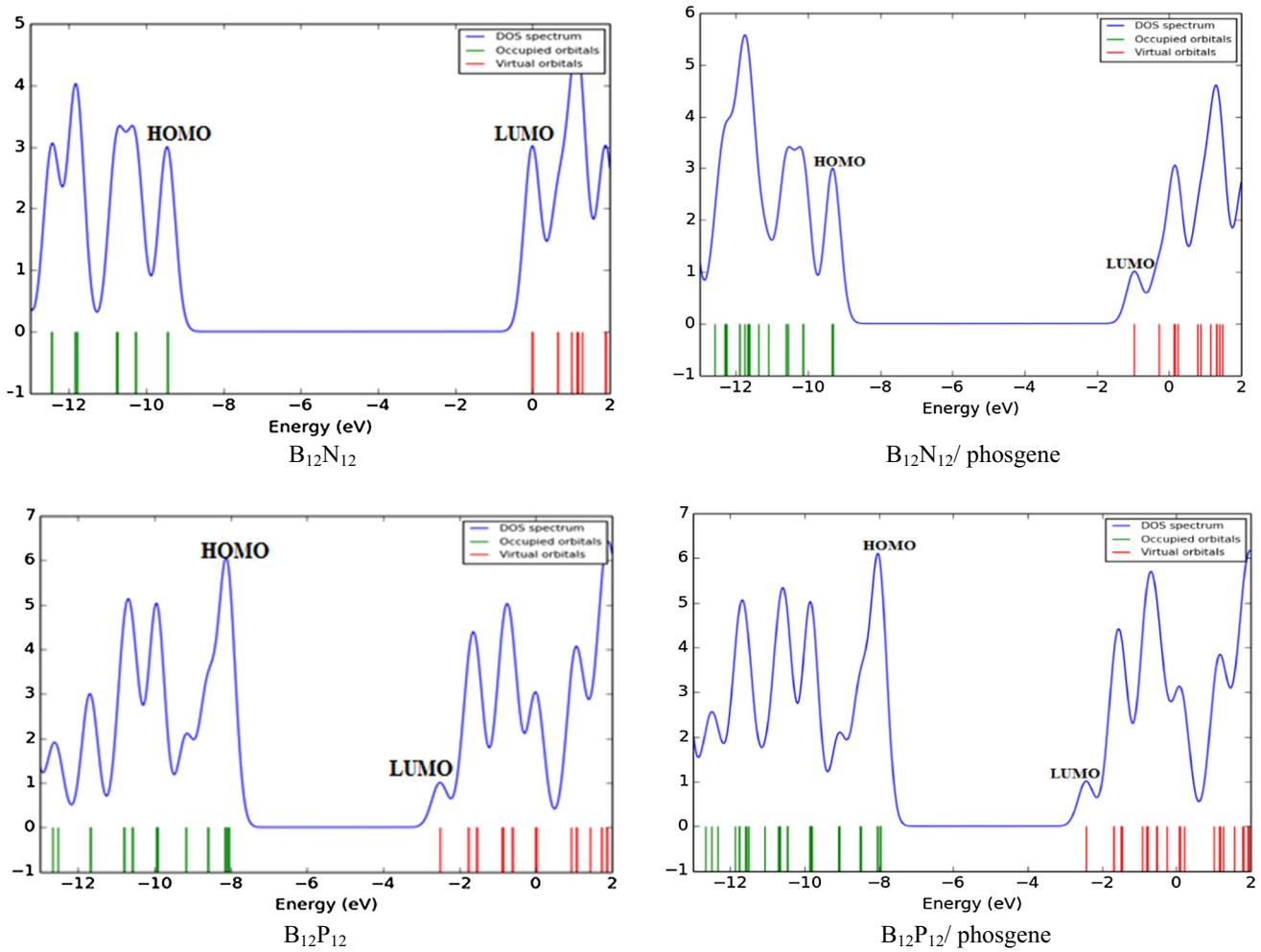

Fig. 5 continued

electrophilic indexes for $Al_{12}N_{12}$ and $B_{12}N_{12}$, but lower electrophilic indexes for $Al_{12}P_{12}$ and $B_{12}P_{12}$ nanoclusters. This is due to the large distance of the phosgene molecule and the nanoclusters.

Figure 4 depicts the HOMO and LUMO distributions of nanocluster/phosgene complexes. Upon the adsorption of phosgene on the exterior surface of nanoclusters close to the Fermi level, there is seen to be significant change in the location of the HOMO and LUMO distribution in all nanoclusters. In spite of these changes in HOMO and LUMO profiles, the E_g values of terminal nanocluster complexes are not significantly altered. The main reason that the E_g values do not undergo significant changes is that there are similar shifts in the position of the HOMO and LUMO orbitals during adsorption.

During the interaction of the phosgene molecule on the exterior surface of all relaxed nanoclusters, some slight alteration in the HOMO and LUMO profiles is observed. The energy of the HOMO and LUMO orbitals and the difference between the HOMO and LUMO orbitals (band gap) for $Al_{12}N_{12}$/phosgene (and $Al_{12}P_{12}$/phosgene) and $B_{12}N_{12}$/phosgene (and $B_{12}P_{12}$/phosgene) nanocluster/phosgene complexes are − 7.67, − 2.18, 5.49 (and − 7.77, − 3.00, 4.77) and − 9.30, − 0.96, 8.34 (− 7.96, − 2.43, 5.53) eV respectively.

With adsorption of phosgene molecules on the outer surface of all pristine nanoclusters, the E_g values of all systems changed significantly. The decrease in the E_g values of the nanocluster/phosgene complexes following complexation corresponds to an increase in conductivity, which is significant for the design of an electrochemical sensor.

The adsorption energies of phosgene molecules on the exterior surface of pure $Al_{12}N_{12}$, $Al_{12}P_{12}$, $B_{12}N_{12}$ and $B_{12}P_{12}$ nanoclusters are − 0.816, − 0.272, − 0.272 and − 0.272 eV, with optimum distances of 2.01, 3.77, 2.52 and 3.42 Å respectively. The adsorption of phosgene molecules on the outer surface of $B_{12}N_{12}$ nanocage performed by Shakerzadeh et al. [7], which fully matches with the results of our research team. They obtained the amount

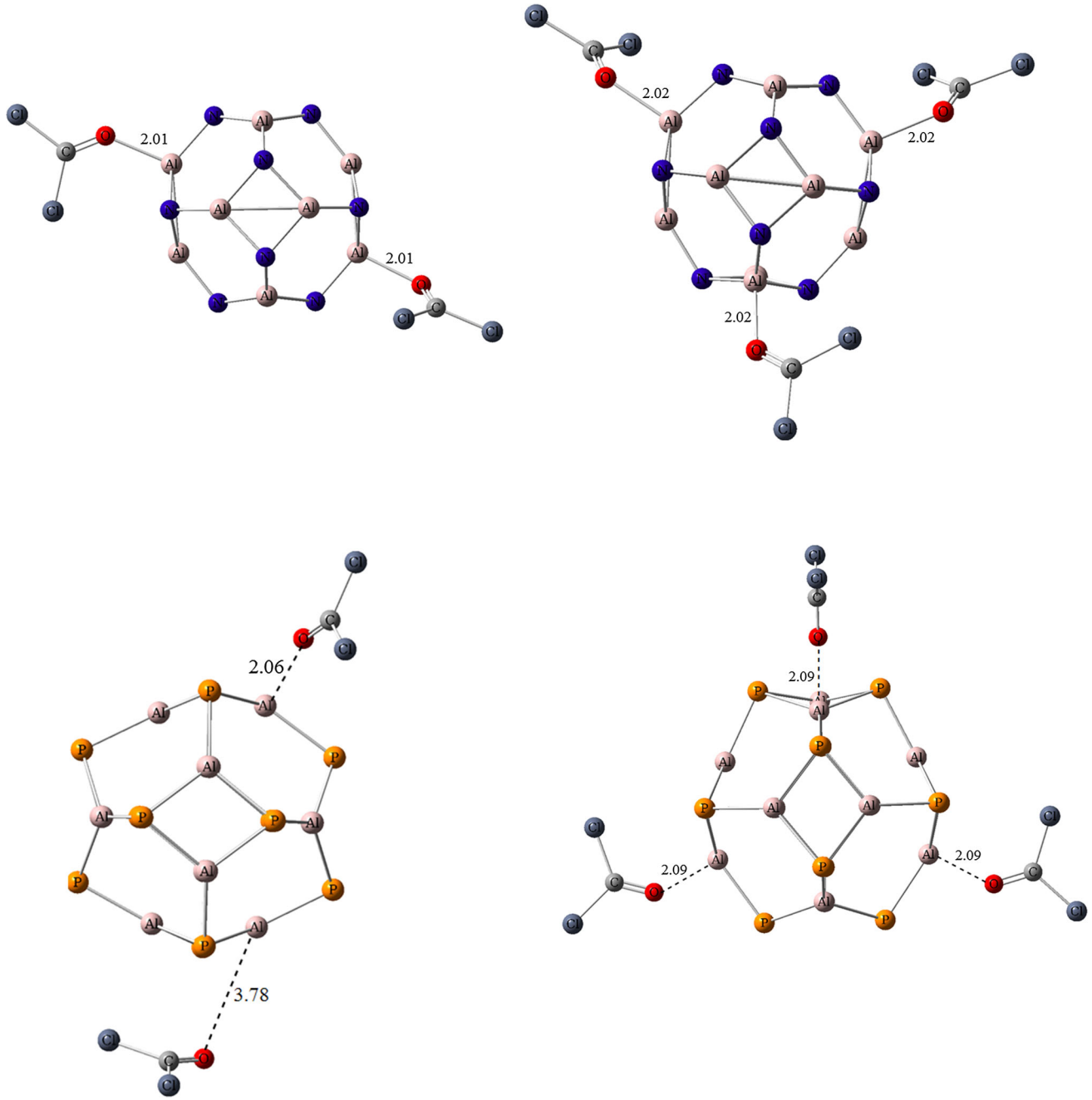

Fig. 6 Optimized structures of 2 and 3 phosgene molecules adsorbed on the Al12N12, Al12P12, B12N12 and B12P12 nanoclusters. Distances are in Å

of absorption energy for this complex of − 0.27 eV that has an excellent correlation with our result. Also, Baei et al. [3] investigated the ability of $Al_{12}N_{12}$ nanocage as a potential sensor for phosgene detection using B3LYP functional and standard 6-31G* basis set, in which those results indicates there is a good correlation with our result.

The above results suggest that the adsorption of phosgene molecules on the $Al_{12}N_{12}$ nanocluster proceeds by way of chemisorption. On the other hand, the small adsorption energies of phosgene molecules on the outer surface of $Al_{12}P_{12}$, $B_{12}N_{12}$ and $B_{12}P_{12}$ pure nanoclusters suggest physisorption. The powerful adsorption of phosgene on the $Al_{12}N_{12}$ nanocluster depends on the greater charge density on the Al atom compared with the B atom. The adsorption energy is inversely proportional to the $X_{12}Y_{12}$–phosgene distance.

As well as, the basis set superposition error (BSSE) was calculated by counterpoise method to delete basis functions

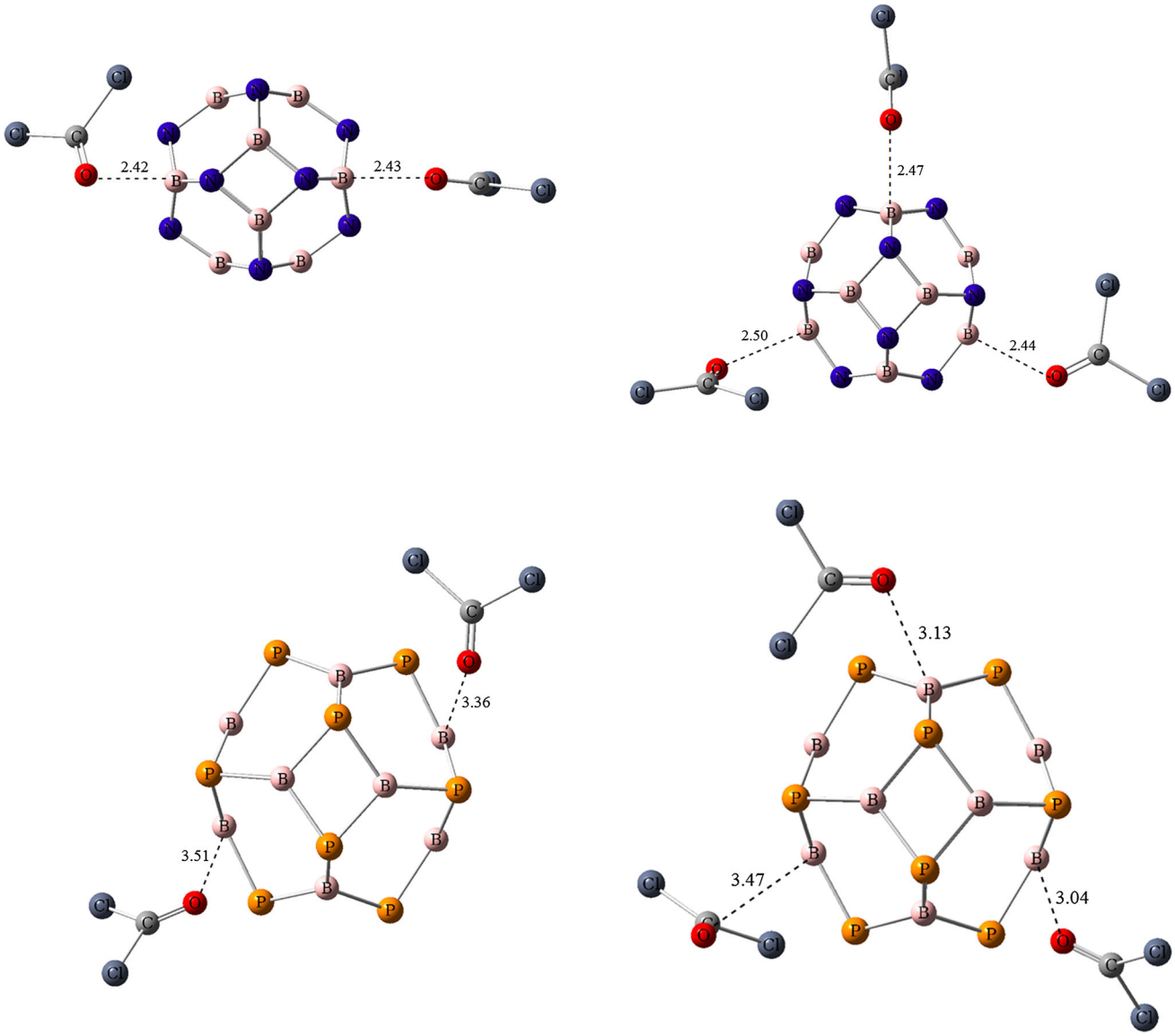

Fig. 6 continued

overlap effects [49]. As shown in Table 2, the E_{BSSE} for $Al_{12}N_{12}$/phosgene (and $Al_{12}P_{12}$/phosgene) and $B_{12}N_{12}$/phosgene (and $B_{12}P_{12}$/phosgene) complexes are 0.195, (and 0.140) and 0.092 (and 0.110) eV, respectively. In Table 2, all methods (M06-2X, B97D and B3LYP) predict that the highest and smallest E_{ads} is achieved for the $Al_{12}N_{12}$/phosgene complex (with a value of − 0.816, − 0.680, − 0.540 eV) and $B_{12}P_{12}$/phosgene complex (with a value of − 0.272, − 0.190, − 0.060), respectively. And the E_g of $B_{12}N_{12}$/phosgene complex is higher than other complexes in all methods ($E_{g,M06-2X}$ = 8.34, $E_{g,B97D}$ = 3.72 and $E_{g,B3LYP}$ = 5.54). In the other word, in comparison with the M06-2X function, the B97D and B3LYP methods underestimate the adsorption energies. This is because of the great displacement of the LUMO state to lower (more negative) energies, so the E_g of the $B_{12}N_{12}$/phosgene nanocluster is increased considerably. It can be concluded that the electronic properties of the $B_{12}N_{12}$ nanocluster are sensitive to the adsorption of phosgene gas. In addition, the B97D and B3LYP methods shown that the binding distance between the adsorbent molecule and the nanoclusters is more than M06-2X. The highest deviation between M06-2X–B97D and M06-2X–B3LYP adsorption energies are 3.11 kcal/mol and 6.37 kcal/mol in the $Al_{12}N_{12}$/phosgene complex, respectively.

Figure 5 shows the electronic density of states (DOSs) of phosgene gas, relaxed nanoclusters and the most stable nanocluster/phosgene complex. Upon the adsorption of phosgene gas on the outer surface of relaxed nanoclusters, the DOSs of all structures is changed. Upon the

Table 3 Calculated thermodynamic data, minimum and maximum vibrational frequencies

Structure	ΔH kJ mol^{-1} K^{-1}	ΔG kJ mol^{-1} K^{-1}	ΔS kJ mol^{-1} K^{-1}	υ_{min} cm^{-1}	υ_{max} cm^{-1}
$Al_{12}N_{12}$/phosgene	308.86	92.45	0.725842697	15.84	1756.66
$Al_{12}P_{12}$/phosgene	250.77	− 55.75	1.028073118	2.97	1890.84
$B_{12}N_{12}$/phosgene	408.44	241.52	0.559852423	4.53	1874.64
$B_{12}P_{12}$/phosgene	300.20	57.21	0.814992453	6.94	18.79.18

adsorption of phosgene molecules on all structures, significant changes can be seen in the location of not only HOMO but also LUMO atomic orbitals, near to the Fermi level, which demonstrate a strong interaction between them. In this work, in spite of the change in location of HOMO and LUMO orbitals, because of the closely similar alterations in the location of HOMO and LUMO orbitals of nanoclusters during interaction with phosgene molecules, the E_g values of all analyzed complexes do not change significantly. Also, during the decoration of $Al_{12}N_{12}$ nanocluster with phosgene, the HOMO orbital moves to larger energy levels, but the LUMO orbital moves to lower energies and is divided into two orbitals. Hence the E_g of this nanocluster increases. In addition, upon interaction of the $Al_{12}P_{12}$ nanocluster with phosgene molecules, the energies of the HOMO and LUMO orbitals are not significantly altered. During the interaction of the $B_{12}N_{12}$ nanocluster with phosgene gas, since the HOMO orbital moves toward higher energy levels and the LUMO orbital moves to lower energies, the E_g of this nanocluster increases. Finally, the occupied and unoccupied states of the $B_{12}P_{12}$ nanocluster do not show a significant change.

Eventually, to obtain the thermodynamic parameters of all $Al_{12}N_{12}$/phosgene, $Al_{12}P_{12}$/phosgene, $B_{12}N_{12}$/phosgene and $B_{12}P_{12}$/phosgene complexes, the alters of ΔH, ΔG, and ΔS of the structures at 298.15 K and 1 atm are calculated and depicted in Table 3. As is shown in Table 3, the calculated value of ΔG for configuration $Al_{12}P_{12}$/phosgene is negative (− 55.75 kJ mol^{-1}), whereas the ΔG value for $Al_{12}N_{12}$/phosgene, $B_{12}N_{12}$/phosgene and $B_{12}P_{12}$/phosgene are 92.45, 241.52 and 57.21 kJ mol^{-1}, respectively. The results indicate that complex $Al_{12}P_{12}$/phosgene is very more stable than others. Also, the ΔH value for the all complexes is positive, demonstrating that the process is endothermic and the process may occur nonspontaneous at room temperature and 1 atm.

Effect of Concentration

At the end of this study, we investigated the effect of the concentration of phosgene gas on the adsorption energy, interaction energy and the sensitivity of the $Al_{12}N_{12}$, $Al_{12}P_{12}$, $B_{12}N_{12}$, and $B_{12}P_{12}$ nanoclusters. To achieve this objective, 2 and 3 phosgene molecules were adsorbed on the outer surface of all nanoclusters, as shown in Fig. 6.

The results (Table 4) show that by increasing the quantity of $COCl_2$ gas the adsorption energy per gas molecule is made less negative (except in the case of

Table 4 Energies of HOMO and LUMO and HOMO–LUMO gap (E_g) in eV, and change of E_g upon adsorption of 1, 2, and 3 $COCl_2$ molecules on $Al_{12}N_{12}$, $Al_{12}P_{12}$, $B_{12}N_{12}$ and $B_{12}P_{12}$ nanocages

Structure	E_{ads}	E_{HOMO}	E_{LUMO}	E_g	BSSE(eV)	$\%\Delta E_g$
$Al_{12}N_{12}$	–	− 8.02	− 1.71	6.31	–	–
1st phosgene molecule	− 0.82	− 7.67	− 2.18	5.49	0.195	− 13.0
2nd phosgene molecule	− 1.09	− 7.35	− 2.06	5.29	0.378	− 16.2
3rd phosgene molecule	− 0.65	− 7.11	− 1.87	5.24	0.581	− 17.0
$Al_{12}P_{12}$	–	− 7.81	− 3.02	4.79	–	–
1st phosgene molecule	− 0.27	− 7.77	− 3.00	4.77	0.140	− 1.88
2nd phosgene molecule	− 0.57	− 7.52	− 2.72	4.80	0.343	0.21
3rd phosgene molecule	− 0.77	− 7.01	− 2.19	4.82	0.593	0.63
$B_{12}N_{12}$	–	− 9.44	− 0.01	9.43	–	–
1st phosgene molecule	− 0.27	− 9.30	− 0.96	8.34	0.092	− 11.60
2nd phosgene molecule	− 0.25	− 9.12	− 0.95	8.17	0.190	− 13.40
3rd phosgene molecule	− 0.24	− 9.01	− 0.89	8.12	0.281	− 13.90
$B_{12}P_{12}$	–	− 8.05	− 2.50	5.55	–	–
1st phosgene molecule	− 0.27	− 7.96	− 2.43	5.53	0.110	− 0.36
2nd phosgene molecule	− 0.20	− 7.91	− 2.40	5.51	0.230	− 0.72
3rd phosgene molecule	− 0.23	− 7.90	2.40	5.50	0.234	− 0.90

The adsorption energy (Ead) per $COCl_2$ molecule is in eV

$Al_{12}P_{12}$). This may be due to the steric effect, that is, by increasing the coverage of $COCl_2$ around the nanoclusters, its tendency to accept another molecule is reduced. Interestingly, with an increase in the number of $COCl_2$ molecules on the outer surface of the nanoclusters, the electronic properties of the clusters change significantly. As shown in Table 4, the HOMO and LUMO values of all structures changed in the same direction (moved to higher energies). For all systems, on an increase in the number of $COCl_2$ molecules, the HOMO–LUMO gap decreased (except in the case of $Al_{12}P_{12}$). This demonstrates that the electrical conductivity of the nanoclusters is increased much more under high gas pressure, and a larger electronic signal can be achieved.

Conclusions

The interaction and electronic properties of $COCl_2$ on relaxed $Al_{12}N_{12}$, $Al_{12}P_{12}$, $B_{12}N_{12}$ and $B_{12}P_{12}$ nanoclusters were examined using DFT calculations with the M06-2X method and the 6-31G(d,p) level of theory. It was found that when a phosgene molecule comes near to the outer surface of all pure nanoclusters, it is adsorbed on the Al atom (for $Al_{12}N_{12}$ and $Al_{12}P_{12}$) or B atom (for $B_{12}N_{12}$ and $B_{12}P_{12}$) of the nanocluster. The results show that the interaction of $Al_{12}N_{12}$ and $COCl_2$ ($E_{ads} = -0.816$) is stronger than for other nanoclusters ($E_{ads} = -0.272$). During the adsorption of $COCl_2$ molecules on the pure nanostructures, the HOMO–LUMO energy gap of all nanocluster complexes is decreased, showing that they can generate an electronic signal in the presence of this gas and can be applied in chemical sensors. In addition, the electronic properties are dependent on the number of $COCl_2$ molecules. The results show that with an increase in the concentration of $COCl_2$ gas the adsorption energy is reduced (except in the case of $Al_{12}P_{12}$).

References

1. Q. M. Wang and R. Q. Huang (2000). *J. Organomet. Chem.* **604**, 287.
2. S. A. Cucinell and E. Arsenal (1974). *Arch. Environ. Health* **28**, 272.
3. M. T. Baei, A. Soltani, S. Hashemian, and H. Mohammadian (2014). *Can. J. Chem.* **92**, 605.
4. J. Beheshtian, A. A. Peyghan, and Z. Bagheri (2012). *Sens. Actuators B* **171**, 846.
5. S.-K. Joung, T. Amemiya, M. Murabayashi, R. Cai, and K. Itoh (2005). *Surf. Sci.* **598**, 174.
6. S. Virji, R. Kojima, J. D. Fowler, J. G. Villanueva, R. B. Kaner, and B. H. Weiller (2010). *Nano Res.* **2**, 135.
7. E. Shakerzadeh, E. Khodayar, and S. Noorizadeh (2016). *Comput. Mater. Sci.* **118**, 155.
8. G. G. Esposito, D. Lillian, G. E. Podolak, and R. M. Tuggle (1977). *Anal. Chem.* **49**, 1774.
9. J. Amani, A. Khoshroo, and M. Rahimi-Nasrabadi (2018). *Microchim. Acta.* **185**, 79.
10. A. Khoshroo, L. Hosseinzadeh, A. Sobhani-Nasab, M. Rahimi-Nasrabadi, and H. Ehrlich (2018). *J. Electroanal. Chem.* **823**, 61.
11. J. Beheshtian, M. Kamfiroozi, Z. Bagheri, and A. Ahmadi (2012). *Chin. J. Chem. Phys.* **25**, 60.
12. J. Amani, M. Maleki, A. Khoshroo, A. Sobhani-Nasab, and M. Rahimi-Nasrabadi (2018). *Anal. Biochem.* **548**, 53.
13. M. Aghazadeh, A. A. M. Barmi, and M. Hosseinifard (2012). *Mater. Lett.* **73**, 28.
14. J. Beheshtian, M. Kamfiroozi, Z. Bagheri, and A. Ahmadi (2011). *Physica E* **44**, 546.
15. H. W. Kroto, J. R. Heath, S. C. O'Brien, R. F. Curl, and R. E. Smalley (1985). *Nature* **318**, 162. https://doi.org/10.1038/318162a0.
16. M. Rahimi-Nasrabadi, A. Khoshroo, and M. Mazloum-Ardakani (2017). *Sens. Actuators B* **240**, 125.
17. J. Beheshtian, M. Kamfiroozi, Z. Bagheri, and A. A. Peyghan (2012). *Chin. J. Chem. Phys.* **25**, 60. https://doi.org/10.1088/1674-0068/25/01/60-64.
18. H. R. Naderi, A. Sobhani-Nasab, M. Rahimi-Nasrabadi, and M. R. Ganjali (2017). *Appl. Surf. Sci.* **423**, 1025.
19. W. Kroto, J. R. Heath, S. C. O'Brien, R. F. Curl, and R. E. Smalley (1985). *Nature* **318**, 162.
20. J. Beheshtian, Z. Bagheri, M. Kamfiroozi, and A. Ahmadi (2012). *J. Mol. Model.* **18**, 2653.
21. D. L. Strout (2000). *J. Phys. Chem. A* **104**, 3364.
22. R. Wang, D. Zhang, and C. Liu (2005). *Chem. Phys. Lett.* **411**, 333.
23. A. Shokuhi Rad and K. Ayub (2016). *J. Alloys Compd.* **672**, 161.
24. A. Shokuhi Rad and K. Ayub (2016). *J. Alloys Compd.* **678**, 317.
25. A. Shokuhi Rad and K. Ayub (2016). *Thin Solid Films* **612**, 179.
26. J. Beheshtian, Z. Bagheri, M. Kamfiroozi, and A. Ahmadi (2011). *Microelectron. J.* **42**, 1400.
27. A. Shokuhi Rad and K. Ayub (2016). *Vacuum* **131**, 135.
28. R. Padash, A. Sobhani-Nasab, M. Rahimi-Nasrabadi, et al. (2018). *Appl. Phys. A* **124**, 582. https://doi.org/10.1007/s00339-018-1965-y.
29. A. S. Rad and K. Ayub (2018). *J. Mol. Liq.* **255**, 168.
30. A. Shokuhi Rad (2016). *Heteroat. Chem.* **27**, 316.
31. A. S. Rad and K. Ayub (2017). *Mater. Chem. Phys.* **194**, 337.
32. A. S. Rad and K. Ayub (2017). *J. Mol. Liq.* **238**, 303.
33. A. S. Rad and K. Ayub (2017). *Solid State Sci.* **69**, 22.
34. A. S. Rad (2017). *J. Nanostruct. Chem.* **7**, 207.
35. A. S. Rad (2017). *Can. J. Chem.* **95**, 845.
36. A. Shokuhi Rad, S. Bagheri Novir, S. Mohseni, N. Ramezani Cherati, and A. Mirabi (2017). *Heteroat. Chem.* **28**, 21396.
37. A. S. Rad (2018). *J. Theoret. Comput. Chem.* **17**, 1850013.
38. Y. Zhao and D. Truhlar (2008). *Theor. Chem. Acc.* **120**, 215.
39. Y. Zhao and D. G. Truhlar (2008). *Acc. Chem. Res.* **41**, 157.
40. N. M. O'Boyle, A. L. Tenderholt, and K. M. Langner (2008). *J. Comput. Chem.* **29**, 839.
41. M. J. Frisch, G. W. Trucks, H. B. Schlegel, G. E. Scuseria, M. A. Robb, J. R. Cheeseman, G. Scalmani, V. Barone, B. Mennucci, G. A. Petersson, H. Nakatsuji, M. Caricato, X. Li, H. P. Hratchian, A. F. Izmaylov, J. Bloino, G. Zheng, J. L. Sonnenberg, M. Hada, M. Ehara, K. Toyota, R. Fukuda, J. Hasegawa, M. Ishida, T. Nakajima, Y. Honda, O. Kitao, H. Nakai, T. Vreven, J. A. Montgomery Jr., J. E. Peralta, F. Ogliaro, M. J. Bearpark, J. Heyd, E. N. Brothers, K. N. Kudin, V. N. Staroverov, R. Kobayashi, J. Normand, K. Raghavachari, A. P. Rendell, J. C. Burant, S. S. Iyengar, J. Tomasi, M. Cossi, N. Rega, N. J. Millam, M. Klene, J. E. Knox, J. B. Cross, V. Bakken, C. Adamo, J. Jaramillo, R. Gomperts, R. E. Stratmann, O. Yazyev,

A. J. Austin, R. Cammi, C. Pomelli, J. W. Ochterski, R. L. Martin, K. Morokuma, V. G. Zakrzewski, G. A. Voth, P. Salvador, J. J. Dannenberg, S. Dapprich, A. D. Daniels, O. Farkas, J. B. Foresman, J. V. Ortiz, J. Cioslowski, and D. J. Fox *Gaussian 09, in* (Gaussian Inc, Wallingford, 2009).
42. J. Beheshtian, Z. Bagheri, M. Kamfiroozi, and A. Ahmadi (2012). *J. Mol. Model.* **18**, 2653.
43. E. Shakerzadeh, N. Barazesh, and S. Z. Talebi (2014). *Superlattices Microstruct.* **76**, 264.
44. J. Li, T. He, and G. Yang (2012). *Nanoscale* **4**, 1665.
45. J. Beheshtian, Z. Bagheri, M. Kamfiroozi, and A. Ahmadi (2011). *Microelectron. J.* **42**, 1400.
46. S. Yourdkhani, T. Korona, and N. L. Hadipour (2015). *J. Phys. Chem. A* **119**, 6446.
47. A. S. Rad, A. Mirabi, M. Peyravi, and M. Mirzaei (2017). *Can. J. Phys.* **95**, 958.
48. T. V. Regemorter, M. Guillaume, G. Sini, J. S. Sears, V. Geskin, J.-L. Bredas, D. Beljonne, and J. Cornil (2012). *Theor. Chem. Acc.* **131**, 1.
49. L. Turi and J. J. Dannenberg (1993). *J. Phys. Chem.* **97**, 2488.